Geochemical Journal, Vol. 41, pp. 303 to 321, 2007

Mineralogy and chemistry of cored sediments from active margin off southwestern Taiwan

JU-CHIN CHEN,[1]* C. Y. LO,[1] Y. T. LEE,[1] S. W. HUANG,[1] P. C. CHOU,[1] H. S. YU,[1] T. F. YANG,[2] Y. S. WANG[3] and S. H. CHUNG[3]

[1]Institute of Oceanography, National Taiwan University, Taipei, Taiwan
[2]Institute of Geoscience, National Taiwan University, Taipei, Taiwan
[3]Central Geological Survey, Ministry of Economic Affairs, Taipei, Taiwan

(*Received June 13, 2006; Accepted June 8, 2007*)

The cored sediments sampled by R/V Marion Dufrense are mostly muds consisting mainly of quartz, feldspar, illite, chlorite + kaolinite and calcite. Authigenic carbonates mainly composed of aragonite, calcite, dolomite and associated with Fe-montmorillonite and pyrite occur in core samples collected from station MD-052911 (22°15.6′ N, 119°51.0′ E) at 2137–2140 cm and 2237–2240 cm depth which may be formed via sulfate reduction by CH_4. In general Illite/Quartz intensity ratios of the sediments show little variation with core depth indicating the relatively constant abundance of illite in the source rock on Taiwan. The cored sediments have higher average Al_2O_3, $\sum$FeO and MgO but lower SiO_2, Na_2O, and CaO contents when compared with upper continental crust (UCC). High field strength elements (Zr, Hf, Y, Nb and Ta) are also depleted in the cored sediments. CaO, Sr, Mn and Pb in the core samples collected from station MD-052912 (22°21.5′ N, 119°48.5′ E) tend to decrease with depth which may be essentially related to the decrease of biogenic $CaCO_3$ with core depth. The La/Th, La/Sc, Th/Sc ratios of the cored sediments are similar to those of UCC, however the $(La/Yb)_N$ ratios of the cored sediments are higher. The cored sediments display similar REE patterns with LREE enrichment and negative Eu anomaly reflecting a felsic nature of the source rock which can also be identified in the La–Th–Sc plot. The chemistry of the sediments can be deduced using a mixing model involved four end members i.e., shale, greywacke, quartzite and limestone.

Keywords: cored sediments, mineralogy and chemistry, active margin, off SW Taiwan

INTRODUCTION

Taiwan Island located at the junction of the Ryukyu and Luzon Arcs in the northwestern Pacific, was formed by the oblique collision between the Luzon Arc and the Chinese continental margin in Late Cenozoic about 5 Ma (Biq, 1997; Suppe, 1981; Ho, 1988). South of Taiwan, the South China Sea lithosphere is subducting eastward under the Luzon arc. East of Taiwan, the Philippine Sea plate is subducting northward under the Ryukyu arc.

Liu *et al*. (1997) concluded that the structural grain of the Taiwan mountain belt trends NNE-SSW, forming an arc convex toward the Asian continent. The orogenic structural features are well demonstrated by a series of stacked folds and thrust sheets verging west (Ho, 1982) on Taiwan. These orogenic structural features are believed to extend southward to offshore southwestern Taiwan (e.g., Letouzey and Sage, 1988; Liu *et al*., 1997).

The Central Geological Survey of the Ministry of Economic Affairs of Taiwan sponsored a comprehensive geophysical, geological and geochemical survey in the area offshore southwestern Taiwan (Fig. 1) where previous geophysical data indicated that bottom simulating reflectors (BSRs) are widely distributed and that gas hydrates may exist in the continental slope of the South China Sea and the accretionary wedge near southern Taiwan (Liu *et al*., 1999, 2004; Schnurle *et al*., 2002). Chi *et al*. (1998) suggested that the area with BSR distribution off southwestern Taiwan may exceed 20,000 square kilometers. The objectives of this study are to present mineralogical and chemical data in the cored sediments in order to shed some light on the source of these sediments. In addition the nature of the sediments and its relationship with the potential occurrence of gas hydrate in the study area will be discussed.

GEOLOGICAL SETTINGS

Taiwan offers a typical example of present-day arc-continent collision between the Luzon arc of the Philippine Sea Plate and the Chinese continental margin. Suppe

*Corresponding author (e-mail: jcchen@oc.ntu.edu.tw)

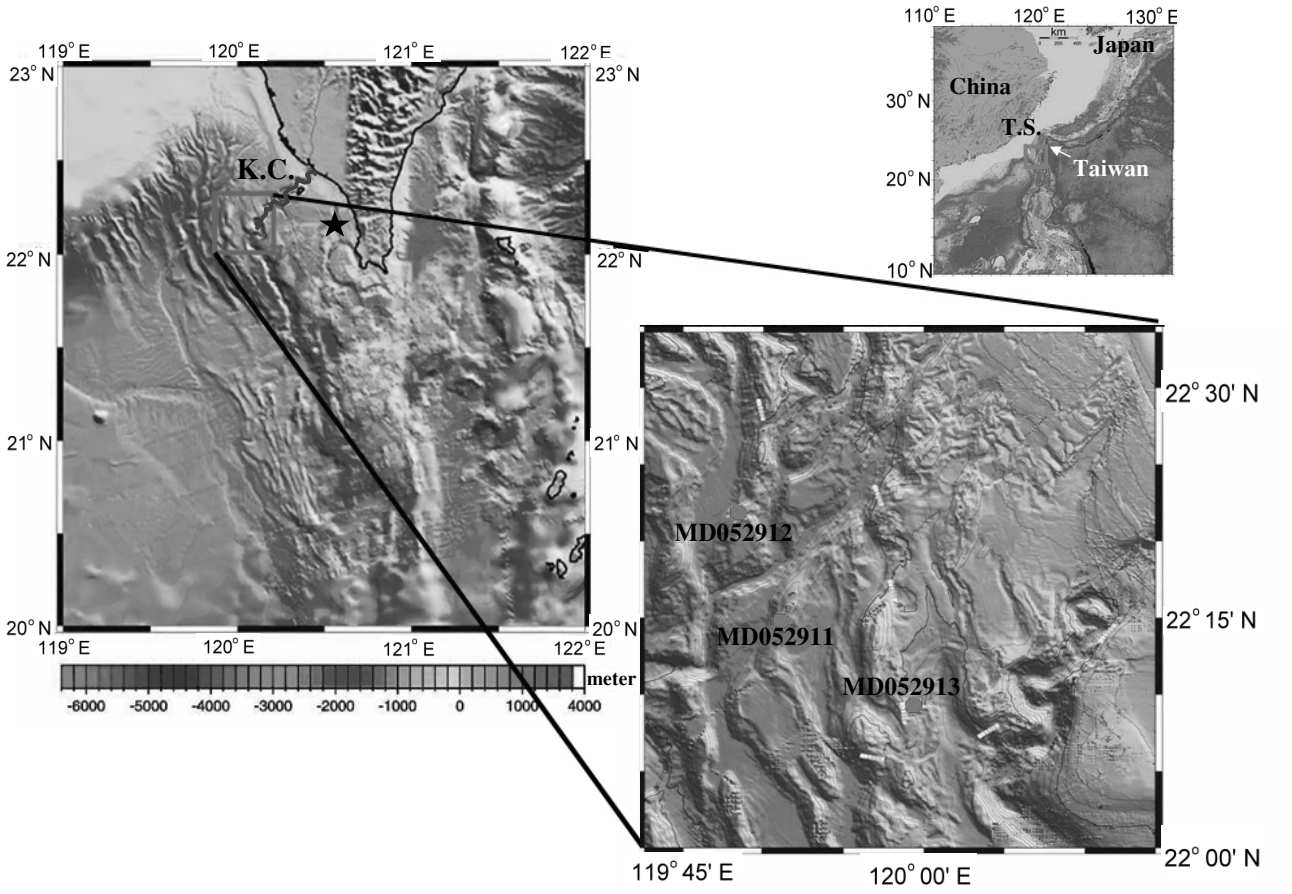

Fig. 1. Location map showing the study area and the coring sites. T.S., Taiwan Strait; K.C., Kaoping Canyon; star indicates the coring site offshore Fanshan, southern Taiwan (Lee, 1987).

(1984) concluded that the collision, flipping and back-arc spreading have been propagating along the continental margin at essentially identical rates since the late Pliocene. The active and relict accretionary wedges on both sides of Luzon are interpreted as resulting from two changes in the direction of subduction by the Luzon arc (Bowin *et al*., 1978).

Tectonically, south of 23°N, including Southern Taiwan and offshore areas are considered in the incipient collision zone. The Pingtung Plain of Taiwan and the Kaoping shelf and slope region are subjected to contraction due to collision between the Luzon arc and the Chinese margin indicated by west-vergent thrust faults and folds. On the other hand, rift-extension dominates in the Chinese margin immediately west of the Kaoping slope as evidenced by the absence of flexural extension normal faults in the Pliocene-Quaternary sediments (Yu and Huang, 2006).

The rock sequence of Taiwan Island is readily divisible into a pre-Tertiary basement and Cenozoic cover more than 10 km thick. The basement outcrops in the form of a 240-km-long inlier on the eastern flank of the Central Range, and consists mainly of a schist-marble complex with minor amounts of ortho- and paragneisses and amphibolites. The Cenozoic sequence covering the basement can be divided into a Central Range Group and a Foothill Zone Group. The former group is a succession principally of slate and phyllite with subordinate quartzite exposed mainly on the crest and west flank of the Central Range, while the latter group is a late Tertiary and Quaternary record of recurrent marine transgressions and regressions consisting of a marine sandstone-shale-mudstone sequence interrupted by three Miocene coal-bearing formations.

The cover succession of western Taiwan is in the form of a prism tapering westward from 8000 m thick in the Foothill Zone, thinning rapidly to only 500 m on the Penghu Islands in the Taiwan Strait (Biq *et al*., 1985). Previous studies (Covey, 1984; Yu and Chou, 2001; Lin and Watts, 2002) suggested that the foreland basin west of the Taiwan mountain belt was formed during Pliocene as the flexural response to the loading of the Taiwan

orogen on the edge of the eastern Chinese margin.

Pliocene-Quaternary sediments more than 5000 m thick derived from the Taiwan orogen have filled the foreland basin (Yu and Chou, 2001). The foreland basin west of Taiwan formed earlier in northern Taiwan and then propagated southward along the spike of the Taiwan orogen, resulting in a mature foredeep in the north and a youthful one in the south (Covey, 1984; Brusset *et al*., 1999; Chiang *et al*., 2004).

The study area is located on the continental slope west of the Kaoping Canyon (Fig. 1) where an active accretionary wedge containing a widely distributed bottom simulating reflector exists. The wide occurrence of BSR together with venting phenomena observed by deep-sea camera using WHOI's TowCam system in October 2005 (Lin, 2006, personal communication) strongly indicate the occurrence of gas hydrates in the study area. High CH_4 contents were found in the pore gas of the obtained core samples in this area which generally increase with core depth (Chuang *et al*., 2006). The $\delta^{13}C$ of CH_4 gases range from –54.4 to –95.0‰ and the $\delta^{13}C$ of CO_2 ranges from –11.6~–29.9‰ (Chuang *et al*., 2006), indicating that an organic gas source predominates at shallower depth; however some thermogenic gases may be introduced from deeper sources. The $\delta^{13}C$ of the authigenic carbonates from the core samples collected in this area is between –47‰ to –55‰, indicating the influence of CH_4 (Huang *et al*., 2006) which is significantly different from the biogenic carbonates found in the same core. In addition, the correlation plot of $\delta^{13}B$ vs. Cl/B indicates that boron in the pore waters is strongly influenced by desorption of exchangeable boron while bottom water boron is affected by a unknown mechanism which may be related to the presence of gas hydrate (Chao and You, 2006). It should be noted that Lin *et al*. (2006) concluded that sulfate showed various degree of depletion in the study area with rapid depletion as shallow as about 2 meters below the sediment/water interface.

Analytical Methods

The sediments were sampled by the giant corer "Calypso" on board R/V Marion Dufrense of the French Polar Research Institute in May, 2005. Cored samples obtained at three stations i.e., MD-052911, MD-052912 and MD-052913 were analyzed in this study. The basic data for the sampling stations including longitude, latitude, water depth, core length and the general descriptions of the cores are given in Table 1.

Mineral identification of bulk sediments was carried out by X-ray diffraction on a Philips PW 1830 X-ray diffractometer with Cu radiation and Ni filter. Sediment samples were washed three times with distilled water by a centrifuge to remove sea water and dried in the oven at

Table 1. General description of the cores

Station	Core recovery (cm)	Latitude	Longitude	Water depth (m)	Description
MD052911	2389	22°15.617′ N	119°51.079′ E	1076	Mostly homogeneous grey mud, locally with foram and shell debris, carbon-bearing materials occur below 1000 cm, authigenic carbonates occur at 2100–2200 cm and 2250–2300 cm which contain aragonite, calcite, dolomite, Fe-montmorillonite and pyrite, also with Pogonophora which live in a reducing environment.
MD052912	3044	22°21.500′ N	119°48.500′ E	1093	Mostly homogeneous grey mud, locally carbon-bearing materials occur (2050–2100 cm). Compaction seems to be stronger below 1000 cm.
MD052913	1268	22°09.156′ N	119°59.284′ E	1095	Mostly homogeneous grey mud, carbon-bearing materials occur at 2050–2100 cm.

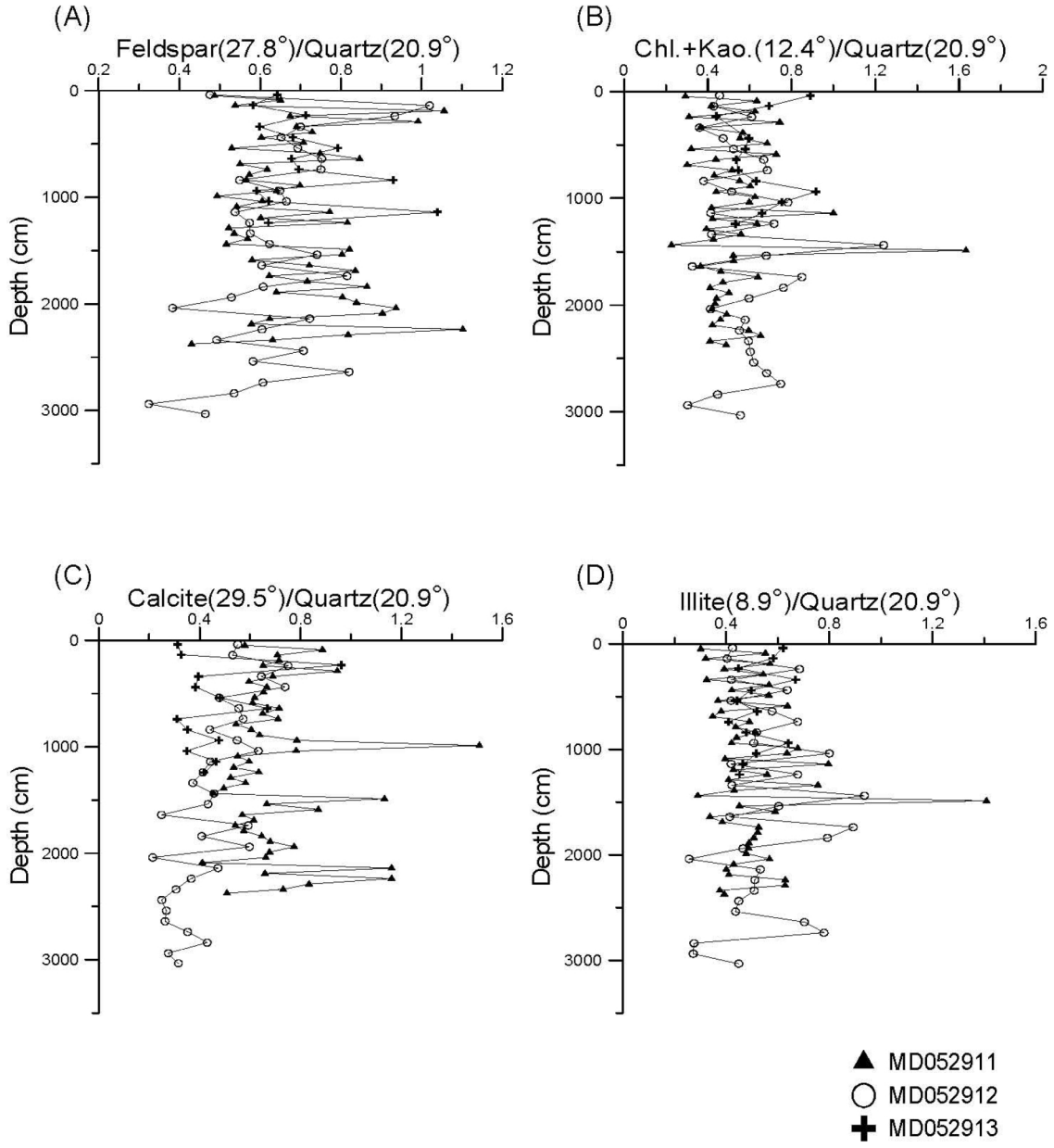

Fig. 2. X-ray intensity ratio variations of constituting minerals with core depth. (A) Feldspar/Quartz, (B) Chl.+Kao./Quartz, (C) Calcite/Quartz, (D) Illite/Quartz.

105°C for 12 hrs. The dried samples were ground into powders with an agate mortar and the powdered samples were dissolved in a mixture of ultrapure HF and HNO_3. Major (except SiO_2) and trace (including REE) elements of the sample solutions were analyzed by ICP-MS at National Tsing-Hwa University using U.S.G.S. standard rocks W-2, BCR-1, AGV-1, GSP-1, G-2 and NBS standards Obsidian and Basalt to draw the calibration curves. The precision for all ICP-MS analyses is estimated better than ±5% of the amounts present, based on replicate analyses of BCR-1. SiO_2 was analyzed by NaOH fusion of sample powers followed by ammonium molybdate colorimetry (Shapiro and Brannock, 1962) using a Shimadzu UV1201 spectrophotometer. Replicate analyses of U.S.G.S. standard rock BCR-1 indicated the precision for SiO_2 analysis is better than ±1.5% of the amounts present.

MINERALOGY OF THE CORED SEDIMENTS

The cored sediments are mostly muds with >4 phi fractions averaging 97% of the total sediments. Mud content shows little variation with core depths. Major minerals

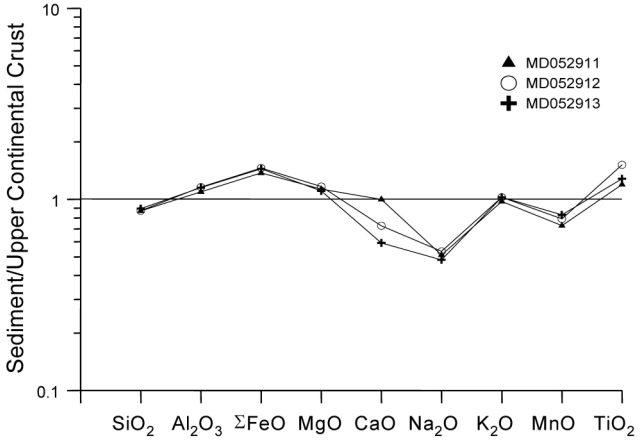

Fig. 3. Average major element contents of the cored sediments normalized to upper continental crust (Taylor and McLennan, 1985).

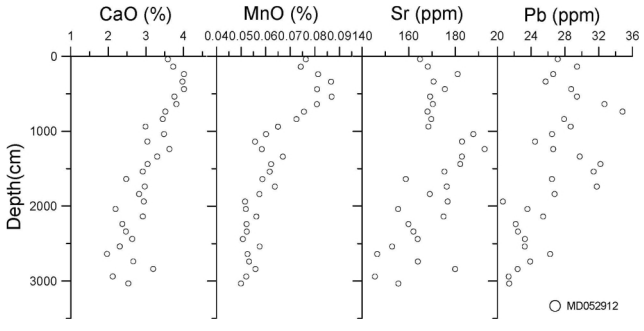

Fig. 4. CaO, Sr, Mn and Pb variations with core depth for MD052912.

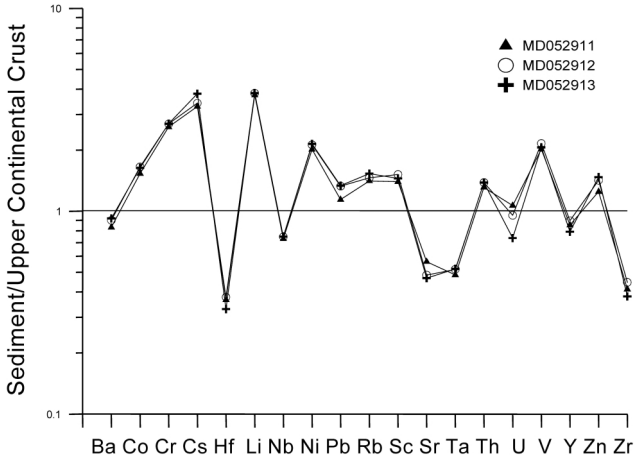

Fig. 5. Trace element contents of the cored sediments normalized to upper continental crust (Taylor and McLennan, 1985).

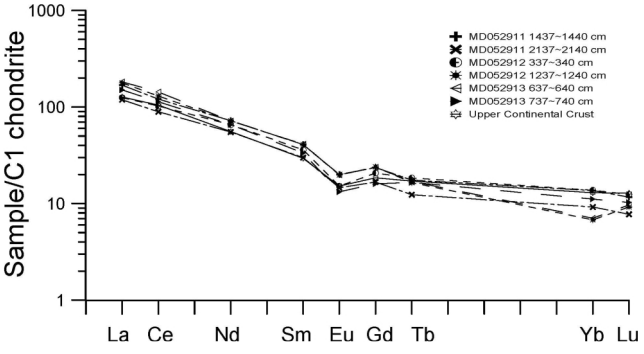

Fig. 6. Chondrite-normalized REE patterns of the cored sediments.

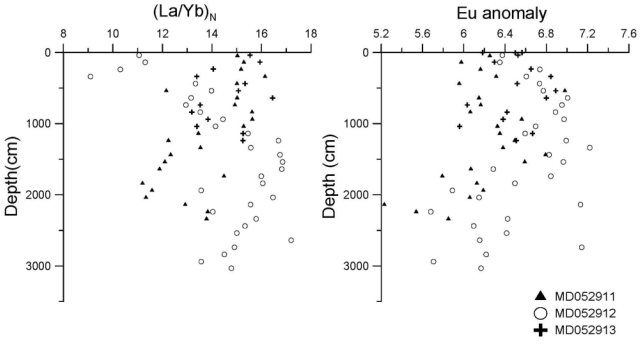

Fig. 7. $(La/Yb)_N$ and Eu anomaly variations with cores depth.

of bulk sediments identified by XRD include quartz, feldspar, illite, chlorite + kaolinite and calcite. In core MD-052911 Feldspar/Quartz intensity ratios are high at certain depths (Fig. 2) which may be related to the mineral components of the source rocks during deposition. In core MD-052912 Calcite/Quartz intensity ratios tend to decrease with core depth due to the decrease of biogenic debris with core depth (Fig. 2).

Special effort was made to search for authigenic carbonates by visual and petrographic investigation because distinct δC^{13} values (–47~–55‰) of bulk carbonates had been found which implied sulfate reduction by methane which could be derived from gas hydrate (Huang *et al*., 2006). Authigenic carbonates were found at 2137–2140 cm and 2237–2240 cm depths in core MD-052911; both showed high Calcite/Quartz intensity ratios (Fig. 2c). XRD analysis indicates that the authigenic carbonates contain essentially aragonite, calcite, dolomite and are associated with Fe-montmorillonite and pyrite. On the other hand, in some core samples the high Calcite/Quartz ratios are related to biogenic debris such as foraminifera, for example at 1000 cm and 1500 cm of core MD-052911. The biogenic carbonates in MD-052911 generally have δC^{13} about –2‰ to –3‰ (Huang *et al*., 2006) which are much heavier than the authigenic carbonate found in the

Table 2. Chemical compositions of the cored sediments. (A) MD-052911.

Sample (cm)	46~49	137~140	237~240	337~340	437~440	537~540	637~640	737~740	837~840
SiO_2 (wt%)	55.73	56.06	57.59	56.98	57.39	55.93	57.05	56.48	57.20
Al_2O_3	17.58	16.76	17.42	17.55	17.28	17.33	16.86	17.38	16.67
∑FeO	6.25	5.98	6.16	6.31	5.96	6.98	6.15	6.16	6.06
MgO	2.49	2.42	2.41	2.42	2.36	2.83	2.31	2.34	2.26
CaO	4.50	4.96	3.67	4.03	3.52	3.86	4.53	4.55	4.02
Na_2O	2.23	2.18	2.23	2.24	2.16	2.11	2.09	2.07	2.04
K_2O	3.37	3.25	3.41	3.38	3.39	3.55	3.35	3.45	3.29
MnO	0.054	0.053	0.051	0.051	0.052	0.075	0.049	0.053	0.049
TiO_2	0.64	0.61	0.63	0.62	0.62	0.61	0.61	0.63	0.61
P_2O_5	0.34	0.21	0.17	0.15	0.23	0.33	0.33	0.25	0.36
L.O.I.	7.39	8.06	7.03	7.11	7.20	7.60	7.69	7.49	7.14
Total	100.586	100.541	100.775	100.834	100.158	101.200	101.013	100.852	99.701
Ba (ppm)	436	410	446	452	454	489	451	474	454
Co	14.8	13.8	14.6	15.0	14.4	17.8	14.4	14.6	13.7
Cr	93	90	93	92	90	101	89	90	89
Cs	11.5	11.2	11.8	11.8	11.8	13.0	11.8	12.1	11.7
Hf	2.05	1.94	1.94	1.82	1.96	2.50	1.87	1.96	1.67
Li	78	74	76	78	77	77	75	75	74
Nb	21.0	19.0	20.3	19.0	19.0	19.1	18.3	19.4	18.6
Ni	40.1	40.5	40.4	40.3	39.8	44.1	36.5	38.1	36.6
Pb	19.7	19.1	20.9	21.2	21.8	25.2	21.1	21.8	20.1
Rb	154	151	158	160	159	168	156	161	155
Sc	16.0	15.2	15.6	15.7	15.4	16.4	15.4	15.6	14.9
Sr	221	231	198	207	193	171	209	218	207
Ta	1.1	1.0	1.1	1.1	1.1	1.1	1.0	1.1	1.0
Th	14.1	13.1	13.8	13.9	13.5	14.9	13.3	13.8	13.0
U	2.84	2.53	2.59	2.61	2.50	2.40	2.53	2.71	2.41
V	129	121	126	124	123	127	123	125	123
Y	18.4	17.4	17.9	17.1	17.5	22.1	17.5	18.0	16.1
Zn	99	87	88	102	130	79	78	82	69
Zr	79	74	76	70	75	93	74	75	65
La	39.6	37.8	39.4	39.5	38.2	38.1	38.0	39.1	37.1
Ce	72.7	70.3	72.1	73.1	70.9	70.5	70.2	72.1	68.5
Nd	32.0	30.7	31.8	32.5	32.0	32.5	31.4	32.5	31.2
Sm	5.8	5.5	5.7	5.9	5.8	6.0	5.8	5.9	5.7
Eu	1.07	1.04	1.08	1.11	1.08	1.14	1.06	1.12	1.06
Gd	4.30	4.14	4.32	4.39	4.44	4.92	4.39	4.39	4.28
Tb	0.58	0.54	0.55	0.56	0.55	0.65	0.56	0.57	0.53
Yb	1.89	1.77	1.86	1.75	1.82	2.25	1.82	1.88	1.70
Lu	0.23	0.23	0.23	0.22	0.23	0.28	0.22	0.23	0.21
Eu/Eu*	0.66	0.67	0.66	0.67	0.65	0.64	0.64	0.67	0.66
$(La/Yb)_N$	15.0	15.3	15.2	16.1	15.0	12.2	15.0	14.9	15.6

$Eu/Eu^* = Eu_n/(Sm_n*Gd_n)^{1/2}$.
$_N$: C1 chondrite normalized (Sun and McDonough, 1989).

same core.

The clay minerals in the mudstones widely distributed in southern Taiwan generally comprise 60~65% illite, 20~30% chlorite and minor to 15% kaolinite of the total clay minerals (Chen, 1973; Chen *et al.*, 2004). Montmorillornite occurs in trace amounts. A similar clay mineral assemblage was found in the Taiwan Strait shelf sediments (Chen, 1973). In general Illite/Quartz intensity ratios show limited variations with core depth (Fig. 2), indicating relative constant I/Q ratios in the source rocks, however this ratio is high at 1500 cm depth in core MD-052911.

Authigenic pyrites are commonly found in the cored sediments (Horng *et al.*, 2004). They can fill into the foraminiferal chambers or replace parts of molluscan shells. In addition, authigenic pyrites can form elongated tubes 2~3 cm long and 0.2~0.3 cm wide which are porous in the center (Huang *et al.*, 2006). Pyrite tubes with similar morphology and size rage were also found in the Hydrate Ridge of the Cascadian margin off Oregon where

Table 2. (continued). (A) MD-052911.

Sample (cm)	937~940	1037~1040	1137~1140	1237~1240	1337~1340	1437~1440	1537~1540	1637~1640
SiO_2 (wt%)	55.15	56.23	57.67	58.27	58.31	55.89	56.04	58.34
Al_2O_3	18.01	17.74	17.15	16.77	16.90	17.17	17.27	16.20
∑FeO	6.56	6.33	6.35	6.49	6.38	6.79	6.59	6.07
MgO	2.42	2.41	2.67	2.66	2.63	2.71	2.81	2.61
CaO	4.62	4.02	3.47	3.57	3.41	3.66	3.84	3.52
Na_2O	2.24	2.07	1.97	1.90	1.96	2.08	2.02	1.87
K_2O	3.54	3.46	3.45	3.39	3.44	3.47	3.52	3.31
MnO	0.054	0.054	0.062	0.069	0.068	0.072	0.080	0.070
TiO_2	0.64	0.64	0.61	0.60	0.57	0.62	0.62	0.57
P_2O_5	0.16	0.23	0.35	0.20	0.22	0.18	0.23	0.19
L.O.I.	7.40	7.48	7.00	6.23	7.14	7.25	7.62	7.59
Total	100.793	100.667	100.749	100.154	101.014	99.895	100.645	100.356
Ba (ppm)	480	471	487	491	488	493	501	472
Co	15.4	15.0	16.4	16.3	16.5	17.3	17.3	16.3
Cr	96	97	101	93	96	97	99	92
Cs	12.4	12.3	12.5	12.4	12.5	12.5	12.8	12.4
Hf	1.96	2.05	2.39	2.49	2.05	2.72	2.72	2.32
Li	77	79	77	76	76	74	76	72
Nb	21.2	20.9	19.4	18.6	17.8	20.0	20.2	17.4
Ni	43.9	39.9	41.7	41.6	41.9	44.1	43.8	41.0
Pb	21.5	21.6	24.4	24.9	24.7	25.3	28.1	24.7
Rb	163	162	165	163	164	164	167	160
Sc	16.3	16.0	15.9	15.8	15.7	16.2	16.5	15.1
Sr	225	202	173	175	163	171	174	161
Ta	1.1	1.1	1.1	1.1	1.0	1.1	1.1	1.1
Th	14.2	13.9	14.7	15.0	14.5	15.5	15.7	14.4
U	2.61	2.62	2.45	2.44	2.09	2.42	2.41	2.22
V	129	128	125	123	121	125	127	117
Y	18.2	18.3	20.5	21.1	19.2	22.5	22.9	20.0
Zn	104	89	81	80	75	93	112	88
Zr	75	78	88	89	76	98	98	82
La	40.8	40.0	39.2	38.3	36.7	39.9	39.9	35.7
Ce	75.5	74.2	72.8	71.2	69.1	73.8	73.7	68.2
Nd	33.1	32.7	32.7	32.7	31.9	33.7	33.9	31.9
Sm	6.0	5.9	6.1	6.2	5.9	6.2	6.3	6.0
Eu	1.14	1.10	1.13	1.14	1.12	1.16	1.16	1.11
Gd	4.40	4.55	4.61	4.80	4.67	4.85	4.93	4.73
Tb	0.57	0.57	0.62	0.64	0.61	0.65	0.68	0.62
Yb	1.87	1.88	2.09	2.24	1.95	2.32	2.37	2.15
Lu	0.23	0.24	0.26	0.27	0.24	0.29	0.29	0.26
Eu/Eu*	0.68	0.64	0.65	0.64	0.65	0.64	0.64	0.64
$(La/Yb)_N$	15.6	15.3	13.5	12.2	13.5	12.3	12.1	11.9

$Eu/Eu^* = Eu_n/(Sm_n*Gd_n)^{1/2}$.
$_N$: C1 chondrite normalized (Sun and McDonough, 1989).

dissociation of gas hydrate was observed (Suess *et al.*, 2001).

CHEMISTRY OF THE CORED SEDIMENTS

The results of the chemical analyses are listed in Table 2. Figure 3 shows the variations of the average values of major elements in the cored sediments (MD-052911, MD-052912 and MD-052913) normalized to upper continental crust (UCC) (Taylor and McLennan, 1985). It is clear that the cored sediments have higher ∑FeO and TiO_2, but lower SiO_2, CaO, Na_2O, MnO and similar K_2O contents when compared with UCC. The relatively higher CaO found in MD-052911 cored sediments (compared with MD-052912 and MD-052913) may be due to the occurrence of biogenic debris and authigenic carbonates.

Figure 4 shows the CaO, Sr, Mn, and Pb of the cored sediments tend to decrease with core depths which may be essentially related to the decrease of biogenic $CaCO_3$ with core depth at MD052912 since Sr, Mn and Pb may

Table 2. (continued). (A) MD-052911.

Sample (cm)	1737~1740	1837~1840	1937~1940	2037~2040	2137~2140	2237~2240	2337~2340	Avg.
SiO_2 (wt%)	59.38	59.53	59.42	59.20	51.47	60.64	61.07	57.4
Al_2O_3	16.27	15.76	15.81	16.15	12.66	15.12	15.82	16.7
∑FeO	5.79	6.13	6.19	6.06	5.23	5.54	5.85	6.2
MgO	2.21	2.56	2.57	2.55	2.66	2.20	2.21	2.5
CaO	3.78	3.23	3.00	3.06	11.07	4.85	4.00	4.2
Na_2O	1.99	1.91	1.93	1.90	1.43	1.67	1.63	2.0
K_2O	3.21	3.24	3.25	3.31	2.47	2.93	3.16	3.3
MnO	0.050	0.063	0.064	0.060	0.043	0.049	0.054	0.058
TiO_2	0.59	0.57	0.56	0.56	0.49	0.56	0.56	0.6
P_2O_5	0.17	0.13	0.16	0.13	0.11	0.11	0.06	0.2
L.O.I.	7.81	7.76	7.60	7.30	12.01	7.08	6.23	7.5
Total	101.234	41.35	41.14	41.08	48.18	40.10	39.57	100.580
Ba (ppm)	453	479	474	475	325	379	450	458
Co	14.3	16.7	16.4	16.1	12.4	13.4	14.6	15.3
Cr	87	88	91	92	70	82	76	91
Cs	11.8	12.7	12.8	13.0	9.9	11.6	13.0	12.1
Hf	1.76	2.59	2.30	2.40	1.63	1.97	1.82	2.12
Li	73	73	75	78	60	68	76	75
Nb	16.8	16.5	15.8	16.6	11.3	16.4	15.2	18.2
Ni	38.4	41.8	41.9	42.9	33.2	35.9	38.8	40.3
Pb	21.3	25.5	24.8	25.0	17.8	21.8	24.7	22.8
Rb	155	161	162	164	106	147	161	158
Sc	14.9	14.7	15.2	15.4	12.1	13.8	14.8	15.4
Sr	197	160	159	161	322	226	206	197
Ta	1.1	1.1	1.1	1.1	0.9	1.1	1.0	1.1
Th	13.2	14.9	14.4	14.8	11.1	13.3	13.7	14.0
U	2.41	2.41	2.35	2.73	9.94	6.45	2.96	2.98
V	117	117	117	117	100	109	116	121
Y	16.4	21.2	20.1	20.3	14.6	16.7	16.6	18.8
Zn	85	87	88	89	68	81	91	89
Zr	66	89	81	82	60	68	65	78
La	35.4	35.3	34.7	35.0	28.2	34.5	34.1	37.3
Ce	66.6	67.7	66.5	67.7	54.6	66.2	65.8	69.7
Nd	31.0	32.2	32.0	32.4	25.7	31.2	31.0	31.9
Sm	5.7	6.0	5.9	5.9	4.6	5.7	5.7	5.8
Eu	1.06	1.13	1.10	1.11	0.85	1.05	1.06	1.09
Gd	4.16	4.74	4.70	4.74	3.44	4.28	4.23	4.47
Tb	0.52	0.64	0.63	0.63	0.46	0.54	0.54	0.58
Yb	1.75	2.26	2.15	2.22	1.56	1.79	1.78	1.96
Lu	0.21	0.27	0.26	0.27	0.19	0.22	0.21	0.24
Eu/Eu*	0.66	0.65	0.64	0.64	0.65	0.65	0.66	0.65
$(La/Yb)_N$	14.5	11.2	11.6	11.3	12.9	13.8	13.8	13.6

$Eu/Eu^* = Eu_n/(Sm_n*Gd_n)^{1/2}$.
$_N$: C1 chondrite normalized (Sun and McDonough, 1989).

replace Ca site in the crystal lattice (Li, 2000). For MD-052911 and MD-052913 no regular chemical variation trends were found with core depth (variation diagrams are not shown here).

The high field strength elements (Zr, Hf, Y, Nb, and Ta) are relatively depleted in the cored sediments (Fig. 5) when compared to UCC (Taylor and McLennan, 1985) which may be related to the abundance of heavy minerals such as rutile and zircon. The chondrite-normalized REE patterns of the cored sediments are shown in Fig. 6. It is apparent that these sediments have similar patterns with light REE enrichment and negative Eu anomaly. The Eu anomaly may reflect the nature of the source rock (McLennan and Taylor, 1991; Awwiller, 1994; Lee, 2002). The $(La/Yb)_N$ and Eu anomaly variations with core depth are shown in Fig. 7. Generally no regular variation trend was found, except that $(La/Yb)_N$ ratios tend to increase slightly with core depths at station MD-052912 which may be due to the occurrence of minor montmorillorite at depth (Jiang *et al.*, 2006).

Table 2. (continued). (B) MD-052912.

Sample (cm)	37~40	137~140	237~240	337~340	437~440	537~540	637~640	737~740
SiO_2 (wt%)	59.08	58.77	57.33	58.43	53.96	54.09	53.50	55.43
Al_2O_3	15.53	15.78	16.39	15.08	17.77	17.90	18.52	18.01
∑FeO	6.37	6.35	6.74	6.61	6.73	6.77	7.01	6.95
MgO	2.62	2.64	2.77	2.57	3.02	2.96	3.11	3.11
CaO	3.58	3.72	4.01	3.97	4.01	3.76	3.81	3.52
Na_2O	1.91	1.95	2.07	1.97	2.27	2.14	2.20	2.18
K_2O	3.15	3.17	3.32	3.18	3.64	3.62	3.75	3.68
MnO	0.076	0.074	0.081	0.087	0.081	0.087	0.081	0.076
TiO_2	0.72	0.72	0.73	0.74	0.85	0.86	0.87	0.76
P_2O_5	0.08	0.14	0.15	0.26	0.23	0.19	0.12	0.15
L.O.I.	7.46	7.56	7.44	7.55	7.51	7.45	7.80	7.03
Total	100.573	100.875	101.024	100.448	100.078	99.824	100.773	100.886
Ba (ppm)	493	494	521	491	515	510	520	506
Co	15.9	15.9	16.4	16.6	17.8	18.4	18.6	18.6
Cr	87	88	77	89	101	108	103	103
Cs	12.5	12.4	13.0	10.5	12.8	12.9	13.8	13.1
Hf	2.38	2.25	2.32	2.56	2.52	2.50	2.70	2.58
Li	67	66	70	65	76	75	79	79
Nb	17.1	17.0	17.1	18.0	18.3	18.9	18.8	17.8
Ni	41.9	42.3	44.5	45.0	45.2	45.9	46.6	46.5
Pb	27.1	29.4	26.6	25.7	28.7	29.4	32.7	34.8
Rb	161	162	167	n.d.	167	166	174	167
Sc	14.3	14.3	14.6	13.9	18.0	17.7	18.7	18.2
Sr	165	168	181	171	175	169	170	168
Ta	1.1	1.0	1.1	1.1	1.1	1.1	1.2	1.1
Th	14.9	14.5	14.5	12.4	15.7	15.8	16.4	15.5
U	1.41	1.34	1.43	1.34	2.87	2.79	3.04	3.09
V	115	115	118	117	135	134	144	137
Y	21.8	21.2	22.1	20.8	22.9	22.4	23.3	22.8
Zn	108	104	101	98	102	104	109	110
Zr	91	89	92	99	101	97	104	98
La	35.0	35.2	34.2	29.6	42.1	43.5	43.1	41.5
Ce	68.6	69.1	68.1	62.5	77.9	87.6	87.6	76.8
Nd	33.6	33.5	35.1	30.6	34.1	35.1	34.2	33.7
Sm	5.9	5.9	6.2	5.5	6.5	6.7	6.6	6.4
Eu	0.91	0.92	0.96	0.88	1.18	1.21	1.19	1.15
Gd	4.18	4.29	4.76	4.25	5.15	5.29	5.09	5.20
Tb	0.69	0.69	0.74	0.69	0.71	0.72	0.74	0.71
Yb	2.27	2.23	2.38	2.33	2.26	2.23	2.35	2.30
Lu	0.31	0.30	0.31	0.31	0.29	0.30	0.31	0.30
Eu/Eu*	0.56	0.56	0.54	0.56	0.62	0.62	0.63	0.61
$(La/Yb)_N$	11.1	11.3	10.3	9.1	13.3	14.0	13.2	12.9

$Eu/Eu^* = Eu_n/(Sm_n*Gd_n)^{1/2}$.
n.d.: not determined.
$_N$: C1 chondrite normalized (Sun and McDonough, 1989).

The ∑REE contents of the cored sediments are higher than UCC (Table 2). The average $(La/Yb)_N$ ratios of the sediments from MD052911, MD052912 and MD052913 ranging from 13.61 to 14.62 (Table 3), are generally higher than the ratio of UCC (9.2). Based on the $(La/Yb)_N$ ratio and the negative Eu anomaly it is suggested that the source rocks of the cored sediments may be felsic (Cullers and Graf, 1983; Cullers, 1995). The average La/Sc, La/Th and Th/Sc ratios of the cored sediments are listed in Table 3. The corresponding ratios of UCC are also listed for comparison. It is clear that these ratios are similar to UCC. Cullers (1994) and Nyakairu and Koeberl (2001) suggested that the variations of La–Th–Sc can be used to distinguish the source rocks for the sediments. In Fig. 8 it is clear that the cored sediments generally fall within the field of mixed sources close to the felsic end member (E in Fig. 8).

In the (K_2O/Na_2O) vs. SiO_2 plots (Fig. 9) the cored

Table 2. (continued). (B) MD-052912.

Sample (cm)	837~840	937~940	1037~1040	1137~1140	1237~1240	1337~1340	1437~1440	1537~1540
SiO_2 (wt%)	55.19	54.39	54.91	56.24	55.27	55.33	53.76	54.52
Al_2O_3	18.07	19.28	18.28	18.73	18.56	18.77	19.62	19.72
∑FeO	6.89	6.97	6.70	6.59	6.99	7.22	6.83	6.96
MgO	3.13	2.96	2.78	2.70	2.63	2.72	2.66	2.70
CaO	3.45	2.99	3.48	3.04	3.62	3.30	3.04	2.92
Na_2O	2.22	2.24	2.22	2.25	2.18	2.03	2.15	2.26
K_2O	3.68	3.85	3.63	3.67	3.65	3.72	3.88	3.89
MnO	0.073	0.065	0.060	0.056	0.058	0.067	0.062	0.062
TiO_2	0.71	0.88	0.86	0.87	0.87	0.88	0.91	0.90
P_2O_5	0.17	0.24	0.17	0.20	0.18	0.22	0.27	0.29
L.O.I.	6.98	6.58	6.99	6.47	6.33	5.74	6.79	6.66
Total	100.552	100.432	100.087	100.814	100.339	99.998	99.968	100.889
Ba (ppm)	521	533	497	513	504	521	527	528
Co	18.4	17.9	16.7	16.4	16.9	16.7	17.4	18.1
Cr	100	104	96	94	96	95	101	105
Cs	13.2	14.0	13.0	13.3	13.2	13.2	13.9	14.0
Hf	2.71	2.38	2.40	2.11	1.87	1.97	1.84	1.77
Li	79	85	82	80	80	80	83	86
Nb	18.8	18.6	18.2	18.8	18.4	18.8	19.5	19.1
Ni	44.9	45.8	44.1	42.0	43.3	n.d.	45.5	47.3
Pb	27.9	28.7	26.5	24.5	26.6	29.8	32.2	31.4
Rb	168	176	165	168	167	168	175	176
Sc	18.1	18.6	17.7	17.7	17.4	17.8	18.3	18.5
Sr	170	168	188	183	193	183	182	175
Ta	1.2	1.2	1.2	1.1	1.1	1.1	1.2	1.2
Th	16.4	15.7	15.2	15.3	14.5	14.7	14.7	14.8
U	3.49	3.43	4.26	3.37	2.66	2.93	2.58	2.64
V	134	143	137	140	136	138	144	144
Y	23.0	21.2	21.1	19.5	17.9	19.6	17.9	17.8
Zn	102	107	119	97	103	120	112	125
Zr	102	93	93	85	77	80	74	73
La	43.2	43.0	42.7	42.7	42.1	42.4	43.0	43.0
Ce	85.3	87.8	84.5	84.9	79.4	84.5	87.2	88.2
Nd	34.7	34.7	34.5	34.7	33.5	34.4	34.5	34.9
Sm	6.6	6.5	6.5	6.4	6.2	6.4	6.4	6.6
Eu	1.18	1.18	1.17	1.18	1.15	1.17	1.17	1.18
Gd	5.26	5.15	4.97	4.97	4.92	5.09	4.91	4.98
Tb	0.72	0.68	0.68	0.66	0.62	0.64	0.63	0.63
Yb	2.29	2.14	2.17	1.98	1.81	1.95	1.84	1.83
Lu	0.30	0.28	0.28	0.25	0.23	0.25	0.23	0.22
Eu/Eu*	0.61	0.62	0.63	0.64	0.63	0.63	0.63	0.63
$(La/Yb)_N$	13.5	14.4	14.1	15.5	16.7	15.6	16.7	16.9

$Eu/Eu^* = Eu_n/(Sm_n*Gd_n)^{1/2}$.
n.d.: not determined.
$_N$: C1 chondrite normalized (Sun and McDonough, 1989).

sediments fall within the active continental margin field which is concordant with the conclusion reached by Yu and Song (1993). It is clear that the variation field of the cored sediments shown in Fig. 9 is different from the northern Taiwan Strait shelf sediments (Chao and Chen, 2003) deposited in a passive margin environment defined by Roser and Korsch (1986). The northern Taiwan Strait shelf sediments are SiO_2 rich generally ranging from 70% to 89% but they are Al_2O_3 poor varying from 4.3 to 12.0%. The MgO, ∑FeO, CaO, Na_2O and K_2O contents in the northern Taiwan Strait shelf sediments are also lower than those found in the cored sediments analyzed in the present study. The La/Th ratios of the northern Taiwan Strait shelf sediments vary from 2.8 to 4.8 which are higher than those found in the cored sediments of the present study (Table 3). The La/Sc ratios of the northern Taiwan Strait shelf sediments ranging from 3.2 to 3.9 are also higher than those found in the cored sediments of the present study (Table 3).

Table 2. (continued). (B) MD-052912.

Sample (cm)	1637~1640	1737~1740	1837~1840	1937~1940	2037~2040	2137~2140	2237~2240	2337~2340
SiO_2 (wt%)	58.11	55.87	56.71	60.25	59.63	58.58	62.47	61.58
Al_2O_3	17.91	18.81	18.36	16.19	17.39	17.83	15.96	16.82
∑FeO	6.29	6.84	6.50	5.89	6.15	7.13	5.68	6.42
MgO	2.50	2.55	2.57	2.21	2.30	2.36	2.08	2.25
CaO	2.47	2.97	2.82	2.94	2.19	2.92	2.37	2.47
Na_2O	2.03	2.11	2.20	1.88	2.06	2.17	1.90	1.97
K_2O	3.54	3.75	3.62	3.29	3.32	3.40	3.17	3.20
MnO	0.059	0.064	0.057	0.052	0.052	0.056	0.052	0.052
TiO_2	0.68	0.88	0.78	0.58	0.90	0.88	0.59	0.70
P_2O_5	0.08	0.16	0.33	0.08	0.37	0.23	0.12	0.19
L.O.I.	6.69	6.68	6.84	6.88	5.79	5.45	6.30	4.77
Total	100.353	100.667	100.787	100.240	100.139	100.997	100.689	100.430
Ba (ppm)	512	525	519	494	470	493	473	464
Co	16.2	18.6	16.4	13.9	15.3	16.1	14.3	16.0
Cr	92	96	99	82	92	94	81	87
Cs	13.4	13.8	13.1	13.0	11.2	12.1	11.6	11.4
Hf	1.68	1.86	1.90	1.76	1.92	2.14	1.82	2.12
Li	75	80	80	73	77	77	72	71
Nb	17.9	18.6	18.0	17.9	19.1	18.5	17.8	18.0
Ni	40.7	43.7	42.8	37.3	40.3	41.7	37.6	39.3
Pb	26.5	31.8	26.8	20.7	23.6	25.4	22.2	22.4
Rb	166	173	166	158	151	158	153	151
Sc	17.3	18.1	17.6	15.0	16.3	17.2	14.3	16.7
Sr	159	176	169	177	155	175	160	162
Ta	1.1	1.1	1.1	1.1	1.2	1.2	1.1	1.1
Th	14.8	15.0	14.7	13.5	14.4	14.7	13.6	14.6
U	2.36	2.94	3.01	2.24	2.64	2.99	2.39	2.94
V	133	141	135	119	125	130	111	124
Y	17.5	18.7	18.5	16.3	17.9	19.2	16.6	18.9
Zn	98	109	104	84	93	107	84	94
Zr	68	75	76	62	77	83	64	82
La	40.6	42.2	41.2	33.3	41.8	42.2	35.0	41.6
Ce	75.7	80.4	77.9	64.8	86.1	86.1	68.5	80.3
Nd	32.8	34.0	33.8	30.9	34.5	34.2	32.4	33.3
Sm	6.2	6.4	6.4	5.7	6.5	6.4	5.9	6.2
Eu	1.13	1.14	1.14	1.06	1.18	1.14	1.09	1.11
Gd	4.52	4.94	4.88	4.16	4.93	4.76	4.56	4.48
Tb	0.60	0.62	0.62	0.53	0.64	0.63	0.57	0.61
Yb	1.73	1.89	1.84	1.76	1.82	1.95	1.79	1.89
Lu	0.22	0.23	0.23	0.21	0.22	0.25	0.22	0.25
Eu/Eu*	0.65	0.62	0.63	0.67	0.64	0.63	0.64	0.64
$(La/Yb)_N$	16.8	16.0	16.1	13.6	16.5	15.6	14.0	15.8

$Eu/Eu^* = Eu_n/(Sm_n*Gd_n)^{1/2}$.
$_N$: C1 chondrite normalized (Sun and McDonough, 1989).

CONTRIBUTIONS OF DIFFERENT SOURCE ROCKS AND THE MIXING MODEL

From the La–Th–Sc plots (Fig. 8) it is clear that the cored sediments were derived from mixed sources. As mentioned above, the Foothill Zone of Taiwan consists mainly of sandstone, shale and mudstone with minor amounts of limestone which are the potential source rocks for the cored sediments. Since detailed chemical compositions of these potential source rocks are not available at present, we select four end members i.e., shale, greywacke, quartzite and limestone (Table 5) from the literature (Govindaraju, 1989; Condie, 1993; Meisel *et al.*, 1990) to deduce the percentage of contributions of different source rocks using a mixing model designed by Ho and Chen (1996).

The computer model was designed to use all constituting elements to find out the percentages of contribution of each end member by linear regression analysis based on the following equation:

Table 2. (continued). (B) MD-052912.

Sample (cm)	2437~2440	2537~2540	2637~2640	2737~2740	2837~2840	2937~2940	3031~3034	Avg.
SiO_2 (wt%)	59.10	60.26	59.66	57.95	58.50	63.95	60.14	57.51
Al_2O_3	17.33	17.08	18.32	17.69	17.73	15.36	17.20	17.61
∑FeO	6.10	6.42	6.15	7.14	6.22	5.71	6.17	6.56
MgO	2.33	2.29	2.26	2.21	2.35	2.03	2.24	2.57
CaO	2.63	2.30	1.96	2.66	3.19	2.12	2.53	3.06
Na_2O	2.14	1.98	2.11	2.01	2.07	1.75	2.02	2.08
K_2O	3.31	3.28	3.62	3.43	3.40	2.96	3.33	3.49
MnO	0.051	0.058	0.053	0.053	0.056	0.052	0.050	0.063
TiO_2	0.88	0.87	0.67	0.65	0.67	0.60	0.65	0.78
P_2O_5	0.18	0.16	0.19	0.17	0.16	0.09	0.25	0.19
L.O.I.	6.34	5.89	5.80	5.76	6.90	5.94	6.26	6.60
Total	100.383	100.587	100.786	99.738	101.240	100.554	100.851	100.516
Ba (ppm)	472	461	485	466	464	431	451	496
Co	15.5	15.9	15.8	15.9	15.6	14.1	15.9	16.5
Cr	92	90	97	96	97	83	95	94
Cs	11.5	11.4	13.1	12.5	11.7	10.9	11.6	12.6
Hf	2.30	2.33	1.74	2.22	2.45	2.36	2.21	2.18
Li	73	73	79	79	78	70	76	76
Nb	18.8	18.9	21.5	20.9	21.0	18.0	20.2	18.7
Ni	40.0	40.7	41.0	39.9	41.4	37.9	39.9	42.5
Pb	23.3	23.2	26.2	23.9	22.4	21.3	21.4	26.6
Rb	155	152	172	163	160	147	156	164
Sc	17.0	16.7	16.0	15.7	15.8	13.9	15.3	16.7
Sr	164	153	146	164	180	145	156	169
Ta	1.2	1.2	1.2	1.2	1.2	1.1	1.1	1.1
Th	15.1	14.8	14.6	14.6	14.9	14.3	14.1	14.8
U	3.24	3.04	2.12	2.38	2.73	2.66	2.43	2.67
V	128	125	128	126	127	109	123	129
Y	20.2	20.0	16.9	18.7	20.4	18.3	18.7	19.7
Zn	100	95	95	91	95	81	77	101
Zr	90	90	68	83	93	81	85	85
La	43.1	43.0	41.6	41.5	42.5	37.5	40.7	40.5
Ce	84.9	86.4	79.8	82.0	87.6	71.7	81.2	79.8
Nd	34.7	34.8	33.8	33.5	34.1	34.2	33.4	33.9
Sm	6.3	6.5	6.1	6.1	6.2	6.3	6.1	6.3
Eu	1.16	1.15	1.13	1.14	1.16	1.14	1.14	1.12
Gd	4.78	4.90	4.44	4.61	4.82	4.76	4.70	4.80
Tb	0.64	0.65	0.58	0.60	0.61	0.61	0.59	0.65
Yb	2.01	2.05	1.73	2.00	2.10	1.99	1.97	2.03
Lu	0.26	0.26	0.22	0.25	0.26	0.24	0.24	0.26
Eu/Eu*	0.64	0.62	0.66	0.66	0.65	0.63	0.65	0.63
$(La/Yb)_N$	15.3	15.0	17.2	14.9	14.5	13.6	14.8	14.3

$Eu/Eu^* = Eu_n/(Sm_n * Gd_n)^{1/2}$.
$_N$: C1 chondrite normalized (Sun and McDonough, 1989).

$$S = \alpha A + \beta B + \gamma C + \delta D + \varepsilon$$

$$A = \sum_{j=1}^{n} W_{A(j)} \bullet X_j$$

$$B = \sum_{j=1}^{n} W_{B(j)} \bullet X_j$$

$$C = \sum_{j=1}^{n} W_{C(j)} \bullet X_j$$

$$D = \sum_{j=1}^{n} W_{D(j)} \bullet X_j .$$

Where S represents elemental concentration of each sample;

Table 2. (continued). (C) MD-052913.

Sample (cm)	37~40	134~137	242~244	337~340	437~440	537~540	637~640	737~740
SiO_2 (wt%)	60.23	59.98	58.75	56.93	59.56	55.93	55.81	62.31
Al_2O_3	17.53	17.71	17.35	17.77	17.15	18.98	19.25	15.81
∑FeO	6.53	6.30	6.65	6.84	6.52	6.89	6.80	6.03
MgO	2.39	2.38	2.50	2.67	2.62	2.74	2.70	2.12
CaO	2.03	2.02	2.66	3.04	2.76	2.68	2.67	2.05
Na_2O	1.86	1.84	2.01	1.96	1.97	1.80	1.99	1.62
K_2O	3.52	3.55	3.46	3.62	3.45	3.80	3.81	3.12
MnO	0.067	0.063	0.072	0.073	0.073	0.073	0.070	0.061
TiO_2	0.61	0.61	0.59	0.61	0.59	0.87	0.88	0.56
P_2O_5	0.20	0.24	0.24	0.20	0.20	0.14	0.20	0.01
L.O.I.	5.63	5.76	6.60	6.56	6.43	5.85	6.08	6.08
Total	100.595	100.447	100.884	100.280	101.325	99.758	100.260	99.780
Ba (ppm)	507	512	531	507	496	519	520	484
Co	16.7	15.8	17.3	17.9	17.5	18.4	17.5	13.8
Cr	91	90	91	95	94	103	102	81
Cs	14.4	14.7	14.2	14.4	13.5	14.3	14.2	14.4
Hf	1.73	1.66	1.84	2.10	1.96	2.18	2.02	1.72
Li	77	80	80	83	77	84	84	65
Nb	19.6	19.3	18.6	19.3	16.8	19.4	19.4	16.8
Ni	40.9	40.3	44.1	46.4	43.9	45.9	45.3	36.6
Pb	30.0	29.2	28.8	28.3	26.0	26.3	28.9	23.8
Rb	176	180	174	177	165	178	175	160
Sc	15.6	15.9	15.7	16.2	17.3	18.3	18.2	13.9
Sr	148	151	172	178	170	171	170	149
Ta	1.2	1.2	1.2	1.1	1.1	1.2	1.1	1.1
Th	14.9	14.9	14.7	14.8	15.0	15.6	15.1	14.7
U	2.80	2.19	2.14	2.28	2.44	2.82	2.36	1.46
V	120	121	119	126	128	138	139	112
Y	16.6	15.6	16.7	18.2	17.6	19.4	18.3	16.0
Zn	103	101	n.d.	129	103	103	111	99
Zr	63	60	64	75	74	86	80	67
La	37.3	37.1	35.1	36.7	39.2	42.6	43.2	35.6
Ce	71.6	71.7	68.6	71.2	73.8	87.1	87.6	69.3
Nd	34.5	34.0	34.0	34.3	32.7	34.5	33.5	30.6
Sm	6.2	6.2	6.1	6.3	6.1	6.5	6.3	5.1
Eu	1.2	1.1	1.1	1.1	1.10	1.18	1.15	0.8
Gd	4.6	4.5	4.7	4.8	4.62	4.98	4.88	3.3
Tb	0.58	0.55	0.59	0.60	0.62	0.67	0.63	0.62
Yb	1.72	1.67	1.79	1.97	1.83	2.03	1.88	1.89
Lu	0.21	0.20	0.23	0.24	0.24	0.26	0.24	0.26
Eu/Eu*	0.66	0.66	0.64	0.64	0.63	0.64	0.63	0.57
$(La/Yb)_N$	15.5	15.9	14.1	13.4	15.3	15.1	16.4	13.5

$Eu/Eu^* = Eu_n/(Sm_n*Gd_n)^{1/2}$.
n.d.: not determined.
$_N$: C1 chondrite normalized (Sun and McDonough, 1989).

A, B, C and D represent end members;
α, β, γ and δ denote percentage of contribution of A, B, C and D respectively;
ε denotes deviation, minimum ε is required;
W represents weighting;
j denotes any constituting element;
x denotes "variable".

It should be mentioned that minimum ε is required during the calculation. If we know the chemical compositions of all of the potential source rocks ε should equal to zero. In the model values vs. analytical results plots a perfect fit will display all the data points falling on the 45° slope line.

In order to simplify the mixing model, we assume that the sediments were formed from a single mixing event involving these four end members, which may not be the

Table 2. (continued). (C) MD-052913.

Sample (cm)	837~840	937~940	1037~1040	1137~1140	1238~1241	Avg.
SiO_2 (wt%)	60.89	59.31	62.19	57.01	58.58	59.04
Al_2O_3	17.01	17.02	15.94	18.13	17.89	17.50
∑FeO	6.42	6.38	5.96	6.67	6.51	6.50
MgO	2.30	2.26	2.07	2.49	2.42	2.44
CaO	2.31	2.67	2.11	2.81	2.52	2.49
Na_2O	1.68	2.04	1.80	1.96	1.90	1.88
K_2O	3.37	3.34	3.17	3.59	3.55	3.49
MnO	0.063	0.062	0.055	0.065	0.067	0.066
TiO_2	0.59	0.59	0.57	0.64	0.63	0.64
P_2O_5	0.10	0.10	0.05	0.22	0.28	0.17
L.O.I.	6.20	6.70	6.70	6.79	6.84	6.33
Total	100.936	100.475	100.619	100.374	101.201	100.533
(ppm)						
Ba	519	503	483	496	503	506
Co	15.2	15.1	14.2	16.2	16.8	16.3
Cr	89	88	80	102	118	94
Cs	14.4	13.8	13.3	13.3	13.5	14.0
Hf	1.87	1.73	2.02	2.05	1.90	1.91
Li	71	71	64	79	79	76
Nb	17.7	17.4	17.5	20.8	20.6	18.7
Ni	40.9	42.3	37.5	43.1	50.4	42.9
Pb	25.0	25.8	26.6	23.6	24.6	26.7
Rb	172	168	161	170	171	171
Sc	14.7	14.6	14.3	17.7	16.5	16.0
Sr	163	173	148	172	163	164
Ta	1.1	1.1	1.1	1.1	1.1	1.1
Th	14.5	13.9	14.3	14.9	14.8	14.8
U	1.30	1.30	1.21	2.31	2.20	2.06
V	119	120	112	128	126	124
Y	17.6	17.1	17.1	18.4	17.6	17.4
Zn	102	125	106	93	80	104
Zr	75	70	73	78	72	72
La	35.0	35.1	34.7	40.8	39.5	37.8
Ce	69.5	69.0	67.7	81.6	74.5	74.1
Nd	33.4	32.9	31.0	33.7	32.9	33.2
Sm	5.6	5.7	5.2	6.2	6.0	6.0
Eu	0.9	0.9	0.8	1.14	1.11	1.05
Gd	3.9	3.9	3.4	4.63	4.62	4.37
Tb	0.61	0.59	0.58	0.59	0.57	0.60
Yb	1.91	1.82	1.86	1.92	1.86	1.86
Lu	0.26	0.25	0.25	0.23	0.22	0.24
Eu/Eu*	0.58	0.57	0.61	0.65	0.64	0.63
$(La/Yb)_N$	13.2	13.8	13.4	15.3	15.2	14.6

$Eu/Eu^* = Eu_n/(Sm_n * Gd_n)^{1/2}$.
$_N$: C1 chondrite normalized (Sun and McDonough, 1989).

case in nature. It should be mentioned that a single mixing event involving various end members may reach a similar final composition as a polycycling process. For example a polycycling process involving four end members (i.e., shale, greywacke, quartzite and limestone) may generate final sediments which have bulk chemistry similar to those sediments produced by a single mixing event involving these four end members but with different percentages of contributions based on the following assumption:

Table 3. La/Sc, La/Th, Th/Sc and $(La/Yb)_N$ ratios of the cored sediments as compared with upper continental crust (Taylor and McLennan, 1985)

	MD052911	MD052912	MD052913	UCC
La/Th	2.66	2.73	2.56	2.80
La/Sc	2.43	2.43	2.37	2.73
Th/Sc	0.91	0.89	0.93	0.97
$(La/Yb)_N$	13.6	14.3	14.6	9.2

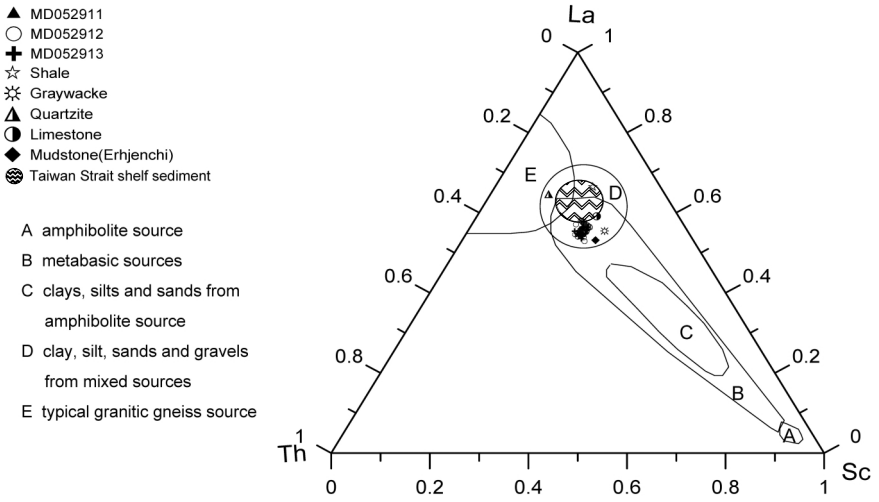

Fig. 8. La–Th–Sc variations for the cored sediments (variation fields modified from Cullers, 1994). The Taiwan strait shelf sediments (Chao and Chen, 2003) are also plotted for comparison. Shale after Govindaraju (1989), greywacke after Condie (1993), quartzite after Meisel et al. (1990), limestone after Govindaraju (1989), mudstone (Erhjenchi) after Chang (1996).

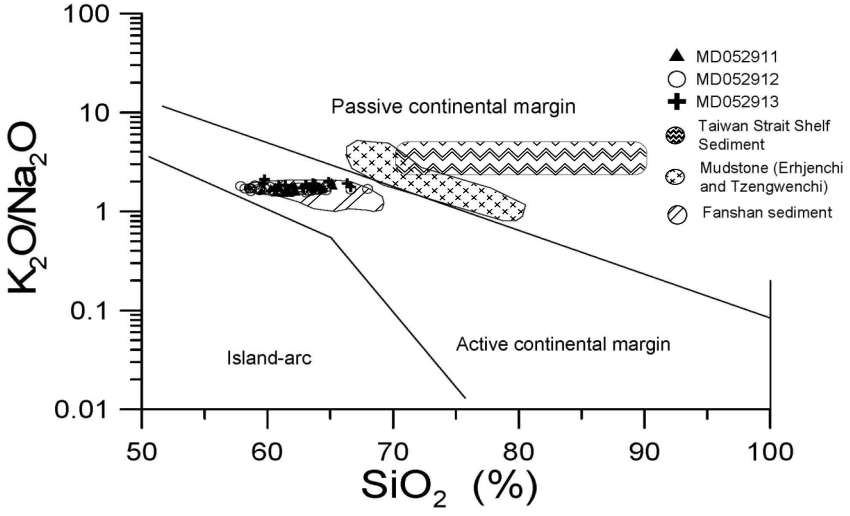

Fig. 9. K_2O/Na_2O vs. SiO_2 plots for the cored sediments (variation field after Roser and Korsch, 1986). Taiwan Strait shelf sediments from Chao and Chen (2003); mudstone (Erhjenchi and Tzengwenchi) from SW Taiwan after Chang (1996); Fanshan sediments after Lee (1987).

$$\vec{S} = [W_1, W_2, W_3] \begin{Bmatrix} S_1 \\ S_2 \\ S_3 \end{Bmatrix} = \begin{bmatrix} \alpha_1 & \beta_1 & \gamma_1 \\ \alpha_2 & \beta_2 & \gamma_2 \\ \alpha_3 & \beta_3 & \gamma_3 \end{bmatrix} \bullet \begin{Bmatrix} A \\ B \\ C \\ D \end{Bmatrix} + \begin{Bmatrix} \varepsilon_1 \\ \varepsilon_2 \\ \varepsilon_3 \end{Bmatrix}.$$

Where S denotes cored samples analyzed;
S_1, S_2 and S_3 represent sediments for (polycycling) process 1, 2 and 3 respectively (all are unknown);
W denotes weighting (i.e., percentage of contribution, all are unknown);
α_1, β_1 and γ_1 represent contributing percentages of end member A, B, C and D respectively (unknown);
A, B, C and D denote four end members (source rocks);
ε denotes deviation.

The calculated results for selected sediments from cores MD-052911, MD-052912 and MD-052913 are shown in Table 5. The calculated chemical compositions based on the mixing models and the analyzed data of the cored sediments are plotted in Fig. 10 in order to test the validity of the models. It is clear that most elements fall close to the 45° slope line indicating that the mixing model

Table 4. Chemical compositions of the end members used in mixing models calculations

	Shale[1)]	Graywacke[2)]	Quartzite[3)]	Limestone[4)]
SiO_2 (wt%)	59.23	66.3	92.7	15.6
Al_2O_3	18.82	15.5	4.18	5.03
∑FeO	6.91	6.2	0.11	2.3
MgO	2.01	2	0.42	5.19
CaO	6.91	3.2	0.06	35.67
Na_2O	0.35	3.1	0.06	0.08
K_2O	4.16	2.3	1.15	0.78
TiO_2	0.66	0.72	0.44	0.33
P_2O_5	0.16	0.14	n.d.	0.05
L.O.I.	5.97	n.d.	n.d.	34.14
Total	98.87	99.46	99.12	99.17
Ba (ppm)	450	650	133	120
Co	21	15	1.1	9
Cr	99	70	86	32
Hf	2.9	3.9	18	1.8
Nb	14.3	10	n.d.	6.6
Ni	36.8	30	5	17.8
Rb	205	100	67	32
Sc	18.50	14.00	3.1	6
Sr	90	280	n.d.	913
Ta	1.00	0.85	1	0.46
Th	12.8	8.5	6.2	4.1
U	1.5	1.8	2.5	1.9
V	87	130	n.d.	36
Y	26.0	28.0	n.d.	9.1
Zr	96	145	634	52
La	62.0	28.0	17	14.6
Ce	109.0	61.0	25.7	25.4
Nd	48.0	26.0	9.8	12
Sm	8.4	4.9	2	2.4
Eu	1.70	0.90	0.4	0.51
Gd	6.70	4.34	n.d.	1.9
Tb	1.02	0.66	0.5	0.35
Yb	2.6	2.2	2.2	0.9
Lu	0.41	0.38	0.4	0.14

[1)]Shale: GSR-5 (Govindaraju, 1989).
[2)]Graywacke: AMCG, average Meso-Cenozoic greywackes (Condie, 1993).
[3)]Quartzite: AQTZ, A-DC quartzite in Tasmania, Australia (Meisel et al., 1990).
[4)]Limestone: GSR-6 (Govindaraju, 1989).

Table 5. Results of mixing model calculations and the percentages of contributions of different end members to the cored sediments

Sample	M-Ex. 1	M-Ex. 2	M-Ex. 3
SiO_2 (wt%)	65.60	66.07	64.21
Al_2O_3	15.71	15.52	15.35
∑FeO	5.94	5.90	5.74
MgO	1.89	1.89	1.96
CaO	4.47	4.23	5.58
Na_2O	1.85	2.01	1.55
K_2O	2.86	2.76	2.90
TiO_2	0.67	0.68	0.65
P_2O_5	0.14	0.13	0.13
Ba (ppm)	533	545	497
Co	16.0	15.6	15.9
Cr	82	80	82
Hf	4.67	4.74	4.83
Nb	10.7	10.5	10.6
Ni	30.3	29.9	29.8
Rb	135	129	137
Sc	14.7	14.4	14.5
Sr	193	203	197
Ta	0.9	0.9	0.9
Th	9.8	9.6	9.9
U	1.75	1.77	1.75
V	103	106	96
Y	24.9	25.0	23.7
Zr	167	170	171
La	39.2	37.3	40.4
Ce	75.1	72.4	75.9
Nd	32.5	31.2	32.9
Sm	5.9	5.7	6.0
Eu	1.14	1.10	1.17
Gd	4.82	4.69	4.79
Tb	0.77	0.75	0.78
Yb	2.34	2.31	2.32
Lu	0.39	0.39	0.39
	Percentage of contribution		
Shale[1)]	35.85	30.20	41.17
Graywacke[2)]	55.43	61.12	45.18
Quartzite[3)]	8.12	8.18	10.04
Limestone[4)]	0.59	0.50	3.61

M-Ex. 1: Mixing Model Example 1, MD052911 137–140 cm.
M-Ex. 2: Mixing Model Example 2, MD052912 237–240 cm.
M-Ex. 3: Mixing Model Example 3, MD052913 1137–1140 cm.
[1)]Shale: GSR-5 (Govindaraju, 1989).
[2)]Graywacke: AMCG, average Meso-Cenozoic greywackes (Condie, 1993).
[3)]Quartzite: AQTZ, A-DC quartzite in Tasmania, Australia (Meisel et al., 1990).
[4)]Limestone: GSR-6 (Govindaraju, 1989).

is acceptable. We fully understand that these calculations are not perfect since some data points are a little far away from the 45° slope line. The calculated results show P_2O_5, Nb and Ni deficiency but HREE and Zr enrichment, which may be related to the deficiency of apatite, Ti-bearing mineral and olivine and the surplus of zircon in the source rocks. It is clear that the percentages of contributions of these four end members to the cored sediments vary from core to core (Table 5). However, greywacke is the dominant contributor (45.18~61.12%) followed by shale (30.20~41.17%). It should be noted that the present model can not evaluate the variation of clay mineral proportions as related to the distance to Taiwan Island (Jiang *et al.*, 2006), since various source rocks (end members) such as shale and greywacke may contain clay minerals although in different proportions.

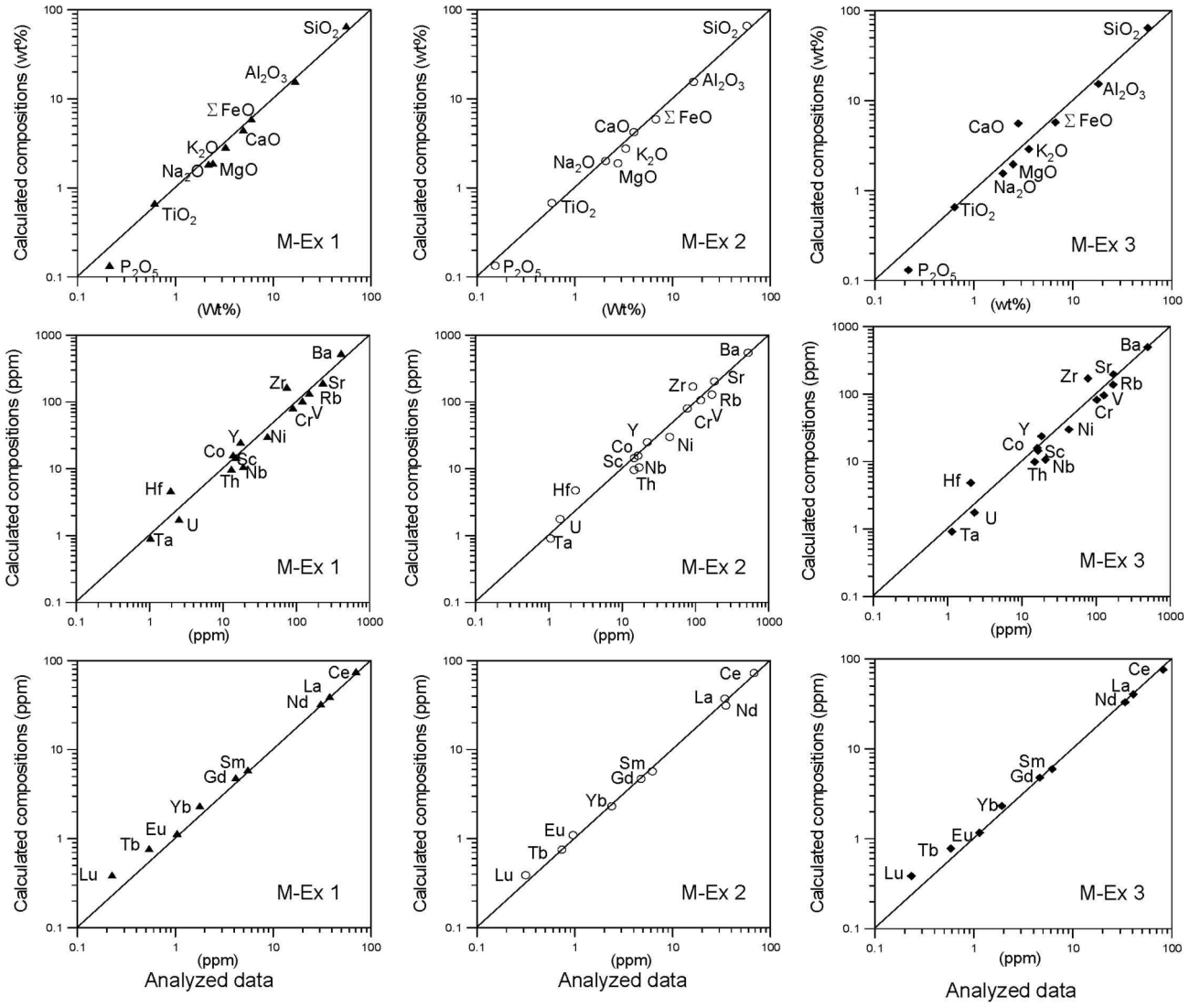

Fig. 10. Calculated chemical compositions vs. analyzed data of the cored sediments to test the mixing models.

CONCLUSIONS

The cored sediments are mostly muds consisting mainly of quartz, feldspar, illite chlorite + kaolimite and calcite. In MD-052912 sediments the Calcite/Quartz intensity ratios tend to decrease with core depth due to the decrease of biogenic debris with core depth. Authigenic carbonates consisting mainly of aragonite, calcite and dolomite associated with Fe-montmorillonite and pyrite occur in core MD-052911 which may be formed via sulfate reduction by methane. In general Illite/Quartz intensity ratios of the sediments show limited variations with core depth which may be due to the relatively constant abundance of illite in the source rock on Taiwan. Authigenic pyrites are commonly found in the cored sediments and form small elongated tubes in some cases.

The average SiO_2, Na_2O, CaO and MnO contents of the cored sediments are generally lower than those of upper continental crust defined by Taylor and McLennan (1985). The high field strength elements (Zr, Hf, Y, Nb and Ta) are also depleted in the cored sediments when compared with UCC. The sediments display similar chondrite-normalized REE patterns with light REE enrichment [$(La/Yb)_N$ ranging from 13.61 to 14.62] and negative Eu anomaly reflecting the felsic nature of the source rocks.

Based on the La–Th–Sc variations the source rocks are deduced to be of "mixed origin", close to the felsic end member. The chemistry of the cored sediments can be deduced by mixing models involving 4 end members i.e., shale, greywacke, quartzite and limestone.

Acknowledgments—We thank Drs. C. S. Liu, S. Lin, C. Y. Huang, C. S. Horng, C. F. You and P. Schnurle for their helpful discussions especially on the selection of sampling sites. Many thanks are given to the caption and crew of R/V Marion Dufresne for their help on sediments sampling. Special thanks are due to Drs. K. Sugitani, Sam Boggs and two anonymous reviewers for their penetrating reviews of the manuscript which improved the paper substantially. This work was supported by the Central Geological Survey of the Ministry of Economic Affairs of the Republic of China under grant 5226902000-05-94-02.

REFERENCES

Awwiller, D. N. (1994) Geochronlogy and mass transfer in Gulf Coast mudrocks (south-central Texas, USA): Rb–Sr, Sm–Nd and REE systematics. *Chem. Geol.* **116**, 61–84.

Biq, C. (1997) Taiwan. *Encyclopedia of European and Asian Regional Geology* (Moore, E. M. and Fairbridge, R. W., eds.), 711–717, Champman and Hall, London.

Biq, C., Shyu, C. T., Chen, J. C. and Boggs, S., Jr. (1985) Taiwan: Geology, geophysics and marine sediments. *Ocean Basins and Margins—Pacific Ocean* (Nairn, A. E. M., Stehli, F. G. and Uyeda, S., eds.), 503–550, Plenum Publishing Co., New York.

Bowin, C., Lu, R. S., Lee, C. S. and Schouten, H. C. (1978) Plate convergence and accretion in Taiwan-Luzon region. *AAPG Bull.* **62**, 1645–1672.

Brusset, S., Deramond, J., Souquet, P., Mouthereau, F. and Deffontaines, B. (1999) Pro-foreland basin system linked to Taiwan mountain building. *Active Subduction and Collision in Southeast Asia: Data and Models, International Conference and 4th France-Taiwan Symposium*, Montpellier, France, Program and Extended Abstract, 67–68.

Chang, Y. D. (1996) Geochemistry of mudstones from Tzengwenchi and Erhjenchi areas, southwest Taiwan. M.S. thesis, National Taiwan University, 76 pp.

Chao, H. C. and You, C. F. (2006) Distribution of B, Cl and their isotopes in pore waters separated from gas hydrate potential areas offshore southwestern Taiwan. *Terr., Atmos. Ocean Sci.* (in press).

Chao, H. J. and Chen, J. C. (2003) Grain size, mineralogical and chemical characteristics of cored sediments from offshore Hsinchu and their geological implications. *Acta Oceanogr. Taiwan.* **41**, 61–96.

Chen, P. Y. (1973) Clay minerals distribution in the sea-bottom sediments neighboring Taiwan Island and northern South China Sea. *Acta Oceanogr. Taiwan.* **3**, 25–64.

Chen, P. Y., Liu, T. C. and Huang, E. (2004) *Minerals of Taiwan*. The Central Geological Survey of Taiwan, 415 pp.

Chi, W. C., Reed, D. L., Liu, C. S. and Lausch, E. (1998) Distribution of the bottom-simulating reflector in the offshore Taiwan collision zone. *Terr., Atmos. Ocean Sci.* **9**(4), 779–794.

Chiang, L. S., Yu, H. S. and Chou, Y. W. (2004) Characteristics of the wedge-top depozone of the foreland basin system in southern Taiwan. *Basin Research* **16**, 65–78.

Chuang, P. C., Yang, T. F., Lee, H. F., Lan, T. F., Lin, S., Liu, C. S., Chen, J. C., Kuo, C. L. and Wang, Y. (2006) Unusual high methane concentration in offshore southwestern Taiwan: preliminary result of gas composition of samples from cruises OR1-697 and OR1-718. *Terr., Atmos. Ocean Sci.* (in press).

Condie, K. C. (1993) Chemical composition and evolution of the upper continental crust: contrasting results from surface samples and shales. *Chem. Geol.* **104**, 1–37.

Covey, M. (1984) Lithofacies analysis and basin reconstruction, Plio-Pleistocene western Taiwan foredeep. *Petroleum Geology of Taiwan* **20**, 53–83.

Cullers, R. L. (1994) The controls on the major and trace elements variation of shales, siltstones and sandstones of Pennsylvanian-Permian age from uplifted continental blocks in Colorado to platform sediments in Kansas, U.S.A. *Geochim. Cosmochim. Acta* **58**, 4955–4972.

Cullers, R. L. (1995) The controls on the major and trace elements evolution of shales, siltstones and sandstones of Ordovician to Tertiary age in the Wet Mountains region, Colorado, U.S.A. *Chem. Geol.* **123**, 107–131.

Cullers, R. L. and Graf, J. (1983) Rare earth elements in igneous rocks of the continental crust: intermediate and silicic rocks—ore petrogenesis. *Rare Earth Element Geochemistry* (Henderson, P., ed.), 275–316, Elsevier, Amsterdam.

Govindaraju, L. (1989) Geostandards. *Special Issue of Geostandards Newsletter*, 1–28.

Ho, C. S. (1988) *An Introduction to the Geology of Taiwan: Explanatory Text for the Geological Map of Taiwan Ministry of Economic Affairs*, Taiwan, 192 pp.

Ho, K. S. and Chen, J. C. (1996) Geochemistry and origin of tektites from Penglei area, Hainan province, southern China. *Journal Southeast Asian Earth Science*, **13**(1), 61–72.

Horng, C. S., Chen, Y. C., Chen, H. H., Yao, C. K. and Lizuka, Y. (2004) Rock magnetism of sediments in gas hydrate potential area off southwestern Taiwan. *Proceedings of 2004 International Workshop on Gas Hydrate Exploration and Exploitation*, 93–101.

Huang, C. Y., Chien, C. W., Li, H. C. and Lizuka, Y. (2006) Investigations on active cold seeps in syn-collision accretionary prism, Kaoping slope off southwestern Taiwan. *Terr., Atmos. Ocean Sci.* (in press).

Jiang, W. T., Chen, J. C., Huang, B. J., Chen, C. J., Lee, Y. T., Lung, C. C. and Huang, S. W. (2006) Mineralogy and physical properties of cored sediments in gas hydrate potential area off southwestern Taiwan. *Terr., Atmos. Ocean Sci.* (in press).

Lee, C. C. (1987) Mineralogy and chemistry of marine sediments from west Philippine Sea, the South China Sea and offshore area of Fanshan. M.S. thesis, National Taiwan University, 88 pp.

Lee, Y. I. (2002) Provenance derived from the geochemistry of late Paleozoic-early Mesozoic mudrocks of the Pyeongan Supergroup, Korea. *Sediment. Geol.* **149**, 219–235.

Letouzey, J. and Sage, L. (1988) *Geological and Structural Map of Eastern Asia*. AAPG, Tulsa, Oklahoma.

Li, Y. H. (2000) *A Compendium of Geochemistry: From Solar Nebula to the Human Brain*. Princeton University Press, 457 pp.

Lin, A. T. and Watts, A. B. (2002) Origin of the west Taiwan

basin by orogenic loading and flexure of a rifted continental margin. *J. Geophys. Res.* **107**, 1029–1048.

Lin, S., Lim, Y., Hsieh, W., Yang, T. F., Liu, C. S., Wang, Y. S., Chung, S. and Huang, C. Y. (2006) Gas hydrate venting phenomena of the southwestern Taiwan continental margin, a perspective from sea floor pictures and sulfate reduction. *Proceedings of 2006 Taiwan Gas Hydrate Workshop*, 35–36.

Liu, C. S., Huang, I. L. and Teng, L. S. (1997) Structural features off southwestern Taiwan. *Mar. Geol.* **137**, 305–319.

Liu, C. S., Shyu, C. T., Schnurle, P., Fu, S. C. and Hsiuan, T. H. (1999) Evaluation of the potentiality for gas hydrate occurrence off southwestern Taiwan. *Proceedings of Workshop on Marine Resources Exploration and Exploitation*, 93–107.

Liu, C. S., Schnurle, P., Chang, H. L., Wang, Y., Chung, S. H. and Hsiuan, T. H. (2004) Geophysical characteristics and geological settings of bottom simulating reflectors offshore southwestern Taiwan. *Proceeding of International Workshop on Gas Hydrate Exploration and Exploitation*, 26–27.

McLennan, S. M. and Taylor, S. R. (1991) Sedimentary rocks and crustal evolution: tectonic setting and secular trends. *J. Geol.* **99**, 1–21.

Meisel, T., Koeberl, C. and Ford, R. J. (1990) Geochemistry of Darwin impact glass and target rocks. *Geochim. Cosmochim. Acta* **54**, 1463–1474.

Nyakairu, G. W. A. and Koeberl, C. (2001) Mineralogical and chemical composition and distribution of rare earth elements in clay-rich sediments from central Uganda. *Geochem. J.* **35**, 13–28.

Roser, B. P. and Korsch, R. J. (1986) Determination of tectonic setting of sandstone-mudstone suites using SiO_2 content and K_2O/Na_2O ratio. *J. Geol.* **94**, 635–650.

Schnurle, P., Hsiuan, T. H., Wang, K. M., Liu, C. S., Reed, D. and Nakamura, Y. (2002) Characteristics of gas hydrate and free gas offshore southwestern Taiwan: A combined seismic reflection/refraction analysis. *Proceedings of Workshop on New Energy (Gas Hydrate) for 21 Century*, 73–87.

Shapiro, L. and Brannock, W. W. (1962) Rapid analysis of silicate carbonate and phosphate rocks. *U.S.G.S. Bull.* **1144-A**, 56 pp.

Suess, E., Torres, M. E., Bohrmann, G., Collier, R. W., Rickert, D., Goldfingr, C., Linke, P., Heuser, A., Sahling, H., Heeschen, K., Jung, C., Nakamura, K., Greinert, J., Pfmannkuche, P., Trehu, A., Klinkhammer, G., Whiticar, M. J., Eisenhauser, A., Teichert, B. and Elvert, M. (2001) Sea floor methane hydrate at Hydrate Ridge, Cascadia margin. *Natural Gas Hydrate Occurrence, Distribution, and Detection* (Paull, C. K. and Dillon, W. P., eds.), AGU Geophysical Monography, **124**, 87–98.

Sun, S. S. and McDonough, W. F. (1989) Chemical and isotopic systematics of oceanic basalts: implications for mantle composition and processes. *J. Geol. Soc. Lond. Spec. Publ.* **42**, 313–345.

Suppe, J. (1981) Mechanism of mountain building and metamorphism in Taiwan. *Geological Society of China Memoir* **4**, 67–89.

Suppe, J. (1984) Kinematics of arc-continent collision flipping of subduction and back-arc spreading near Taiwan. *Geological Society of China Memoir* **6**, 21–23.

Taylor, S. R. and McLennan, S. H. (1985) *The Continental Crust: Its Composition and Evolution*. Blackwell, Oxford, 312 pp.

Yu, H. S. and Chou, Y. W. (2001) Characteristics and development of the flexural forebulge and basal unconformity of western Taiwan foreland basin. *Tectonophysics* **333**, 277–291.

Yu, H. S. and Huang, Z. Y. (2006) Intraslope basin, seismic facies and sedimentary processes in the Kaoping Slope, offshore southwestern Taiwan. *Terr., Atmos. Ocean Sci.* (in press).

Yu, H. S. and Song, G. S. (1993) Submarine physiography around Taiwan and its relation to tectonic setting. *Journal of the Geological Society of China* **36**, 139–156.